Songklanakarin J. Sci. Technol.
43 (6), 1764-1771, Nov. - Dec. 2021

http://www.sjst.psu.ac.th

Original Article

Model-based design of stator winding inter-turn short circuit faults in induction motors♣

Marut Raksa[1, 2*], Kiattisak Sengchuai[1], Anuwat Prasertsit[1], and Nattha Jindapetch[1]

[1] *Department of Electrical Engineering, Faculty of Engineering*
Prince of Songkla University, Hat Yai, Songkhla, 90110 Thailand

[2] *Department of Electrical Engineering, Faculty of Engineering*
Rajamangala University of Technology Srivijaya, Mueang, Songkhla, 90000 Thailand

Received: 17 December 2020; Revised: 18 June 2021; Accepted: 25 June 2021

Abstract

This paper presents modelling and simulation of the inter-turn short circuit fault in stator winding of a three-phase induction motor. The modeling of the induction motor with the inter-turn short circuit fault was efficiently implemented with developed MATLAB software. The investigation results were obtained from test setup of two 0.37 kW and 2.2 kW, 380/220 V squirrel-cage induction motors. The simulation results of the induction motor model were in good agreement with experimental results in the laboratory. The generated fault signals were used to train an artificial neural network (ANN) for inter-turn short circuit fault detection. From the experimental results, the ANN can detect the faults with up to 96 % accuracy. Based on the proposed model, various applications can be developed for fault monitoring and fault detection of induction motors.

Keywords: induction motor, model-based design, stator winding fault, motor current signature analysis, artificial neural network

1. Introduction

Three-phase squirrel cage induction motors are widely used in industrial applications because of their high efficiency, low cost, low maintenance and being rugged. Although induction motors are reliable, they are subjected to some stresses that can cause faults and lead to damage. The most common faults of an induction motor are mechanical or electrical faults. According to The Institute of Electrical and Electronics Engineers (IEEE) and The Electric Power Research Institute (EPRI) the most common fault is bearing fault at 41%, while 37% are electrical stator faults, and 10% are rotor faults; and 22% remain for all other faults (Deeb, Kotelenets, Assaf, Sultan, & Akaysheedept, 2021).

The stator winding inter-turns short circuit fault can irrecoverably damage an induction motor and a production line system. Therefore, monitoring and detection of stator winding short circuit faults has a high priority. The stator winding fault in electrical machines usually starts with a turn-to-turn fault, which is mostly caused by insulation failure. There are many studies on stator winding fault in an induction motor (Gurusamy, Bostanci, Li, Qi, & Akin, 2021; Shifat & Hur, 2020). The inter-turn short circuit fault is one of the many fault modes in an induction motor (Berzoy, Mohamed, & Mohammed, 2017; Meserkhani, Jafari, & Rahi, 2021; Saddam, Ahmed, Aissa, & Ali, 2019).

As a result, induction motor condition monitoring and fault detection is receiving growing interest in the recent years (Verma, Akkulu, Padmanabhan, & Radhika, 2021). Other studies suggest analyzing the air gap flux and the leakage flux that are measured via search coils placed externally on the motor frame (Gurusamy *et al*., 2021; Shaikh, Park, & Lee, 2021). In (Verma *et al*., 2021) an infrared (IR) thermopile sensor array (IRSA) and a Hall-effect sensor array

♣Peer-reviewed paper selected from The 9th International Conference on Engineering and Technology (ICET-2021)
*Corresponding author
Email address: marut.r@rmutsv.ac.th

(HESA) are used. In (Singh, Grant, DeFour, Sharma, & Bahadoorsingh, 2016) different types of signals have been used as inputs to motor fault diagnosis.

However, these effective methods require measured signals in both healthy and fault conditions to train and test for fault characteristics. In the real world, the induction motor in the production line is often unmeasured after completed installation. Therefore, modeling and fault simulation based on nameplate data on the induction motor can resolve this issue.

In this paper, a model-based design approach is used for modeling and simulation of the induction motor with inter-turn short circuit winding fault. The rest of the paper is organized as follows. The modeling of the induction motor is described in Section II, the experimental setup is explained in Section III, and the results are in Section IV. The conclusion is provided in Section V.

2. Theoretical Background

2.1 Motor current signature analysis

The Motor Current Signature Analysis (MCSA) is a popular method for induction motor condition monitoring. The MCSA aims to use spectrum analysis of stator current to identify characteristic harmonic frequencies indicating possible motor faults. The stator winding short-circuit fault produces some harmonics in the stator current around the base frequency. They are given by

$$f_{st} = f_s\left[\frac{m}{p}(1-s)\pm k\right] \tag{1}$$

where S is the slip, f_{st} is the fault harmonic frequency, f_s is power supply frequency, and m is an index integer 1,2,3,..., while k is an index of integer from 1,3,5... and p is the motor pole pair. The current spectrum comparison between healthy and stator short circuit fault is shown in Figure 1. The harmonic frequencies produced by the fault are clearly indicated at 25 Hz, 75 Hz, 125 Hz, and 175 Hz, as expected from (1).

2.2 Modeling of the induction motor

The modeling of the induction motor with help of its defining equations is presented. The modeling can be divided into four types, as illustrated in Figure 2. The categories are circuit models (Lv, Zeng, & Zhou, 2018; Ojaghi & Daliri, 2017) state space models (Accetta, Cirrincione, Pucci, & Sferlazza, 2020; Pucci, 2019) finite-element method (FEM) models (Faiz, Keravand, Ghasemi-Bijan, Cruz, & Bandar-Abadi, 2016; Kocman, & Nowak, 2019) and thermal models (Boglietti, Cossale, Vaschetto, & Dutra, 2018).

Moreover, model-based design plays an important role in monitoring, forecasting and diagnosis of induction motor faults. For the minimalist, the three-phase induction motor consideration will be developed under following conditions.

- Symmetrical two-pole, three-phase winding.
- Iron losses are neglected.
- The flux density is radial in the air gap.
- The permeability of the iron part is finite.
- The slotting effect is neglected.

If phase A is coincident with the q-axis; the transformed voltage quantities V_{qs} and V_{ds} of the induction motor can be represented as in (2) and (3). The DQ model is provided from the stator current from the inter-turn short circuit fault at any level in any single phase of stator. In DQ modelling, the parameters are easily accessible for control, which is not possible without this technique. Therefore, specifications become independent variables in which a change of one parameter does not affect the other specifications. The DQ model is covering both healthy and inter-turn short circuit fault conditions. The induction motor in the state space model with DQ transformation can be represented as follows.

$$v_{qs} = \frac{2}{3}\left(v_{as} - 0.5v_{bs} - 0.5v_{cs}\right) \tag{2}$$

$$v_{ds} = \frac{2}{3}\left(-\frac{\sqrt{3}}{2}v_{bs} + \frac{\sqrt{3}}{2}v_{cs}\right) \tag{3}$$

where

$$v_{as} = V_m \cos\ \omega_e t, v_{bs} = V_m \cos\ \left(\omega_e t - \frac{2\pi}{3}\right),$$

$$v_{cs} = V_m \cos\ \left(\omega_e t + \frac{2\pi}{3}\right)$$

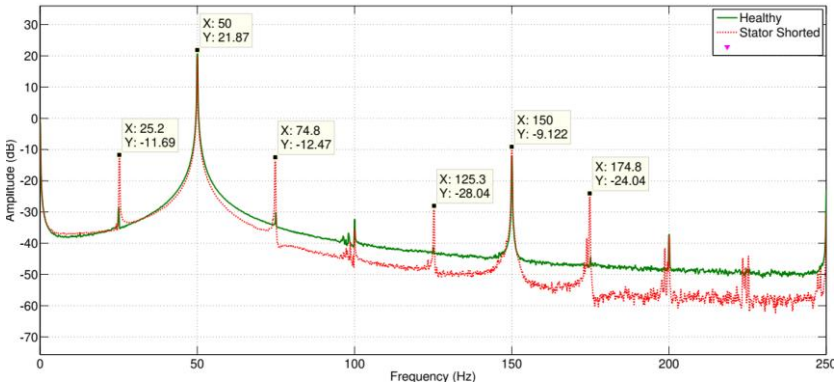

Figure 1. The stator current spectrum when healthy and with inter short circuit faults

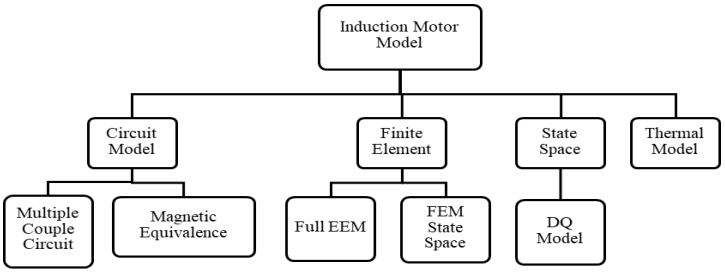

Figure 2. Overview of the induction motor modeling

Figure 3 shows the DQ equivalent circuit of the induction motor. The stator and rotor voltage equations in stationary reference frame are given in equations (4)-(7).

$$\frac{d\lambda_{qs}}{dt} = v_{qs} - i_{qs}r_s \tag{4}$$

$$\frac{d\lambda_{ds}}{dt} = v_{ds} - i_{ds}r_s \tag{5}$$

$$\frac{d\lambda_{qr}}{dt} = -i_{qs}r_r + \omega_r\lambda_{ds} \tag{6}$$

$$\frac{d\lambda_{dr}}{dt} = -i_{ds}r_r - \omega_r\lambda_{qs} \tag{7}$$

Then, the DQ-axis currents are as in (8).

$$\begin{pmatrix} i_{qs} \\ i_{ds} \\ i_{qr} \\ i_{dr} \end{pmatrix} = \begin{pmatrix} l_{ss} & 0 & l_m & 0 \\ 0 & l_{ss} & 0 & l_m \\ l_m & 0 & l_{rr} & 0 \\ 0 & l_m & 0 & l_{rr} \end{pmatrix}^{-1} \times \begin{pmatrix} \lambda_{qs} \\ \lambda_{ds} \\ \lambda_{qr} \\ \lambda_{dr} \end{pmatrix} \tag{8}$$

The induction motor torque can be shown in conditions of the stator currents and flux linkages as in (9).

$$T_e = \frac{3P}{2}(\lambda_{ds}i_{qs} - \lambda_{qs}i_{ds}) \tag{9}$$

The equation of the mechanical movement is (10).

$$\frac{d\omega_r}{dt} = \frac{P}{2J}(T_e - T_l) \tag{10}$$

2.3 Stator inter-turn short circuit modeling

The stator winding of the three-phase induction motor with inter-turn short-circuit on phase B is shown in Figure 4. This is modelling of the inter-turn short-circuit fault. The percentage of shorted turns (μ) is expressed by (11) where n_s is the number of total turns and n_f is the number of shorted turns.

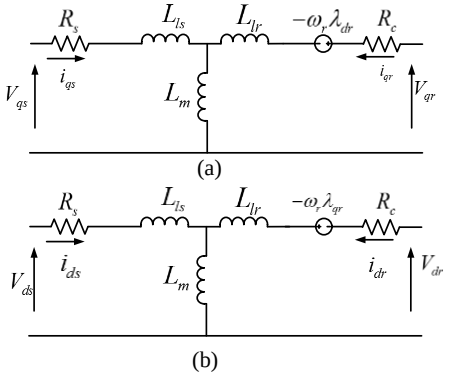

Figure 3. The d-q equivalent circuit of a three-phase induction motor

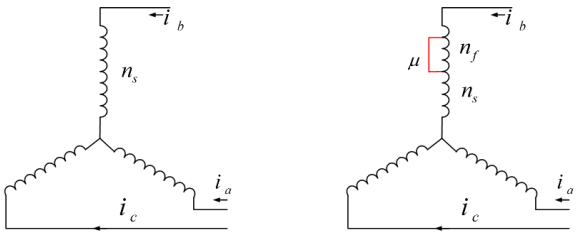

(a) Healthy (b) Inter-turn short-circuits

Figure 4. Three-phase stator winding of the induction motor

$$\mu = \frac{n_f}{n_s} \tag{11}$$

The stator and rotor voltage and flux linkage equations for the inter-turn short circuit induction motor in vector form referred to the stator can be expressed as in (12) - (16).

$$\frac{d\lambda_{qs}}{dt} = v_{qs} - i_{qs}(1-\mu)\,\mathrm{r}_s \tag{12}$$

$$\frac{d\lambda_{ds}}{dt} = v_{ds} - i_{ds}\,\mathrm{r}_s \tag{13}$$

$$\frac{d\lambda_{dsf}}{dt} = \frac{-\mu}{(1-\mu)}\frac{d\lambda_{qs}}{dt} + \mu(\mathrm{r}_s + \mathrm{r}_f)\,\mathrm{i}_{qsf} \tag{14}$$

$$\frac{d\lambda_{qr}}{dt} = -i_{qr}\,\mathrm{r}_r + \omega_r \lambda_{ds} \tag{15}$$

$$\frac{d\lambda_{qr}}{dt} = -i_{ds}\,\mathrm{r}_r - \omega_r \lambda_{qs} \tag{16}$$

The DQ axis currents of induction motor with shorted winding are as in (17).

$$\begin{pmatrix} i_{qs} \\ i_{ds} \\ i_{qr} \\ i_{dr} \\ i_{qsf} \end{pmatrix} = \begin{pmatrix} (1-\mu)^2 l_{ss} & 0 & (1-\mu)l_m & 0 & (1-\mu)l_m \\ 0 & l_{ss} & 0 & l_m & 0 \\ (1-\mu)l_m & 0 & l_{rr} & 0 & \mu l_m \\ 0 & l_m & 0 & l_{rr} & 0 \\ \mu(1-\mu)l_m & 0 & \mu l_m & 0 & \mu^2 l_{ss} \end{pmatrix}^{-1} \times \begin{pmatrix} \lambda_{qs} \\ \lambda_{ds} \\ \lambda_{qr} \\ \lambda_{dr} \\ \lambda_{qsf} \end{pmatrix} \tag{17}$$

The stator current in the model can be decomposed as in (18) and (19).

$$i_{qst} = i_{qs} + \frac{\mu}{(1-\mu)} i_{qsf} \tag{18}$$

$$i_{dst} = i_{ds} + \frac{\mu}{(1-\mu)} i_{dsf} \tag{19}$$

Finally, the torque and speed of induction motor with fault are calculated as in (20) and (21).

$$T_e = \frac{3P}{4}\left(\lambda_{ds} i_{qs} - \lambda_{qs} i_{ds}\right) \tag{20}$$

$$\frac{d\omega_r}{dt} = \frac{P}{2J}\left(T_e - T_i\right) \tag{21}$$

3. Materials and Methods

3.1 MATLAB/SIMULINK model of induction motor with stator winding turn faults.

Based on the DQ model proposed in the previous section, it is possible to simulate variable load level, and stator winding turn faults with different numbers of shorted turns. In MATLAB/Simulink, the system is drawn on the screen as block diagram, shown in Figure 5.

The input block represents the transformation of three phase variables into two phase variables. The DQ block represented by the equations (17) is a transformation of voltage and the induction motor parameters to current and flux. The current-flux to torque-speed conversion is represented by equations (19) and (20). Equation (1) represents the fault harmonic frequency, which is shown in the f_{st} block. In an analysis, equivalent circuits of the motors are used for study and simulation of motors. In the DQ model, the induction motor using the stator voltage equations, the equivalent circuit of the induction motor can be derived, assuming rotor d-axis flux from the induction motor.

3.2 Fault detection using Artificial Neural Network

Artificial Neural Networks (ANN) are among the main tools tested for induction motor fault diagnosis. In this paper, we consider a feedforward multilayer perceptron (MLP) network. Figure 6 shows the diagram of stator fault detection using Artificial Neural Network. The outputs represent phase of the inter-turn shorted circuit fault. In this paper, we used three neurons in the hidden layer. The activation functions of the hidden layer and output layer are hard-limit transfer functions.

For the proposed ANN, the type of network was a multilayer perceptron trained with backpropagation. The outputs of neurons H, A, B and C depend on their weights. The multi-layer feedforward perceptron uses learning cycles (or epochs) where its output is compared with the target or actual output, and the weights are adjusted to decrease deviations iteratively.

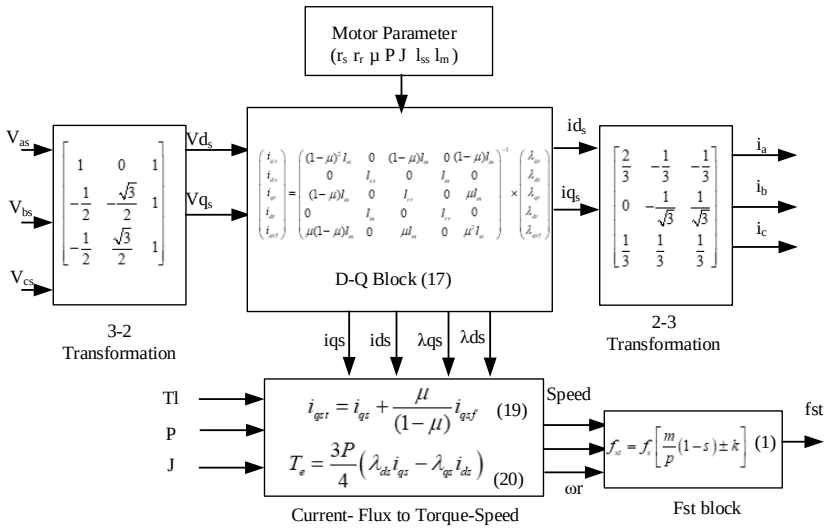

Figure 5. Simulink model of the induction motor with an inter-turn short-circuit

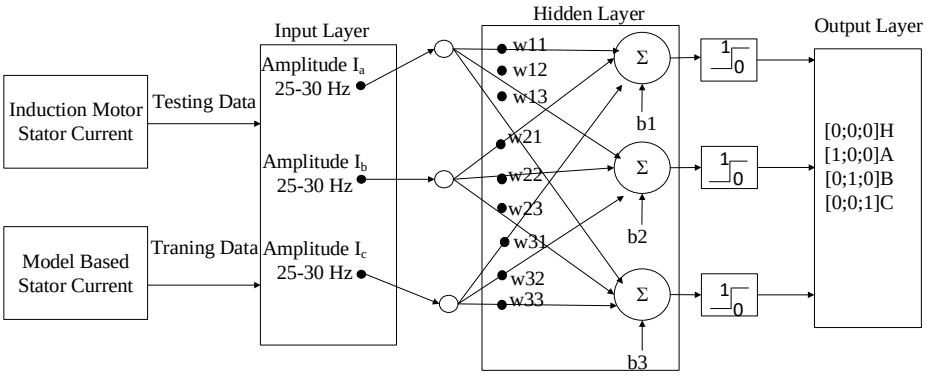

Figure 6. Diagram of the Artificial Neural Network

4. Experimentation and Results

4.1 Experimental setup

In the beginning, an experimental validation of the model is conducted. The induction motor equivalent circuit parameters are shown in Table 1. For validation the proposed DQ model is compared with the experimental results from commercial 0.37 kW and 2.2 kW induction motors. Laboratory experimental setup for both healthy and faulty three-phase squirrel cage induction motor is shown in Figure 7.

The stator currents are collected and prepared for feature extraction, from the current signal of the induction motor. The frequency components and amplitudes of the stator current are efficiently computed with FFT. The proportional amplitudes of harmonic frequency at (1) are carefully compared in the ANN for monitoring the stator winding short turn fault.

The induction motor model here was based on the mathematical equations and the motor specifications of induction motors. As noted above, a successful model for the induction motor typically requires practical inter-turn short circuit fractions (μ). Use of model blocks to import, initialize, and accurately simulate them in MATLAB is described in Figure 5. The induction motor rotor always rotates at a speed less than the synchronous speed. The slip is the difference between the rotor speed (N) and the rotating magnetic flux speed (N_s). The induction motor slip (S) is typically expressed as a percentage of synchronous speed. The induction motor slip (S) is important determinant of the fault harmonic frequency.

The outputs of the induction motor model represent the proportional amplitudes of harmonic frequencies of 25-30 Hz for the ANN training data.

4.2 Experimental validation of the induction motor model

The directly measured machine parameters were carefully compared to the reference signals, and the possible other in common is the accurate estimation of the induction motor parameters. The model parameters and specific variables used in the induction motor model in Table 1 are confirmed by comparison with experimental data from laboratory tests.

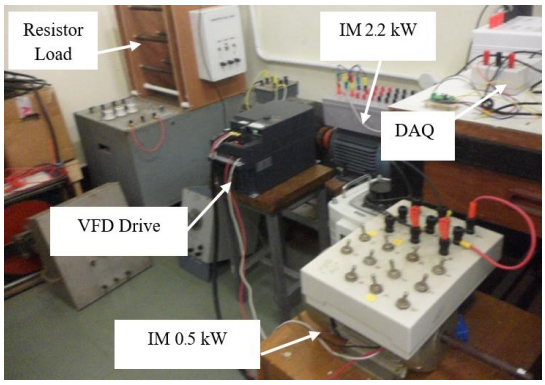

Figure 7. The laboratory setup for induction motor stator short circuit experiments

In order to validate the dynamic model developed, an experimental investigation was also conducted. Table 2 shows the results for comparing experiments with simulation results, for 0.37 kW and 2.2 kW induction motors with 10**%** and 50**%** of their turns shorted.

4.3 Results

The current spectrum comparison between the modeling and testing of induction motor at no-load conditions with 10% inter-turn short circuits is shown in Figure 8.

The harmonic frequency component at 25 Hz in the stator current is the signature for diagnosis of the stator inter-turn shorted circuit fault.

To properly train the neural network, the data set in Table 3 was simulated under different short-turns cases ($\mu = 0$, $\mu = 0.1$ and $\mu = 0.5$) and loading conditions. Table 4 presents the percentage accuracy of classification by the proposed method. The percentage accuracy formula used is given by the actual and simulated amplitude stator currents. Based on comparison between actual and simulated values, we can note that the errors are small. Therefore, Simulink model of the motor can be used to identify the inter-turn short circuit in a three-phase induction motor.

4.4 Discussion

This section discusses the experimental validation of the proposed method. In the model simulation, the current

Table 1. The three-phase induction motor parameters

Parameter	BARNCO71 2-4	ABB M2QA100L4	MULLER OY714
Power (kW)	0.37	2.2	0.37
Voltage (V)	380	380	380
Speed (rpm)	1370	1435	1360
f_s (Hz)	50	50	50
Pole	4	4	4
R_s (Ω)	11.9	2.7	13
l_{ss} (mH)	115.6	28	114
R_r (Ω)	13.4	3.95	14
l_{rr} (mH)	115.6	28	116
l_m (mH)	974	276.3	981
J (kg m^2)	0.0006	0.0067	0.006

Table 2. Comparison between measured and simulated stator currents

Induction motor	μ	I_s Measured	I_s Simulated	Accuracy (%)
BARNCO71 2-4	0	0.755 A	0.725 A	96.02
BARNCO71 2-4	0.1	0.824 A	0.797 A	96.72
BARNCO71 2-4	0.5	0.939 A	0.912 A	97.18
ABB M2QA100L4A	0	2.59 A	2.50 A	96.53
ABB M2QA100L4A	0.1	2.79 A	2.71 A	97.14
ABB M2QA100L4A	0.5	2.92 A	2.84 A	97.27
MULLER OY714	0	2.59 A	2.50 A	96.47
MULLER OY714	0.1	0.79 A	0.77A	97.46
MULLER OY714	0.5	0.91 A	0.89A	97.8

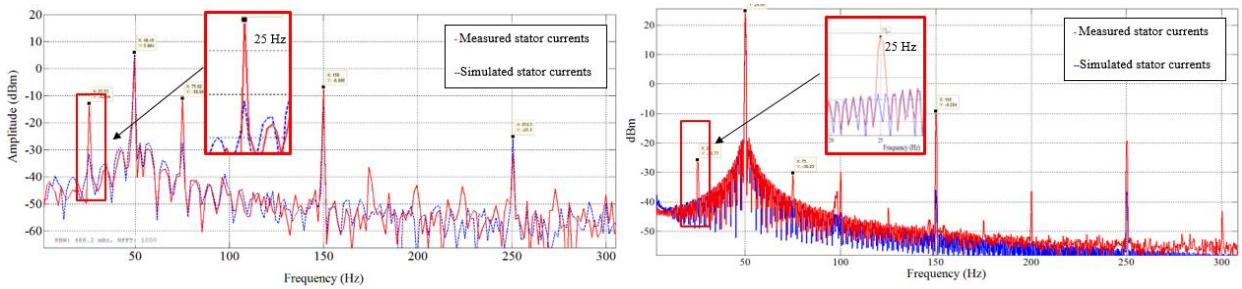

(a) The 0.37 kW induction motor (b) The 2.2 kW induction motor

Figure 8. The current spectrum comparison of the induction motor

Table 4. The accuracy of classification (%) for proposed methods

Motor	BARNCO 0.37 kW			ABB 2.2 kW			MULLER 0.37 kW		
Condition	Healthy	μ=0.1	μ=0.5	Healthy	μ=0.1	μ=0.5	Healthy	μ=0.1	μ=0.5
No Load	93.75	100	100	90	100	100	95	100	100
Half Load	96.87	100	100	96.87	100	100	96.5	100	100
Full load	97.5	100	100	98.1	100	100	96.5	100	100

Table 3. Details of the ANN data sets

Induction motor condition	Training/Testing samples		
	No load	Half load	Full load
Healthy	40/40	40/40	40/40
Phase A Short	40/40	40/40	40/40
Phase B Short	40/40	40/40	40/40
Phase C Short	40/40	40/40	40/40

Note: 160 of the training samples were randomly selected as the validation data.

signals are recorded from typically varying motors conditions and loads with different ratios of stator short circuit turn faults. It was carefully observed that the amplitude of the stator current increased in the practical inter-turn short circuit condition. The simulation results indicate that by analyzing changes in the percentage of winding shorted of the stator, a stator current in the induction motor could be changed. Both graphs indicate a linear correlation between the measured currents and the output from the induction model. Figure 9 shows the magnitude of current in the measured induction motor while a practical inter-turn short circuit fault is emerging. It is applied to varying fractions of winding shorted

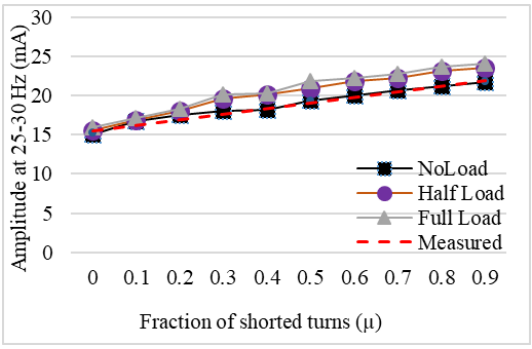

(a) BARNCO 71 2-4 0.37 kW

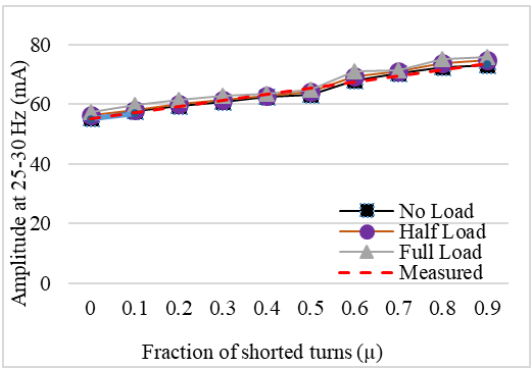

(b) ABB M2QA100L4A

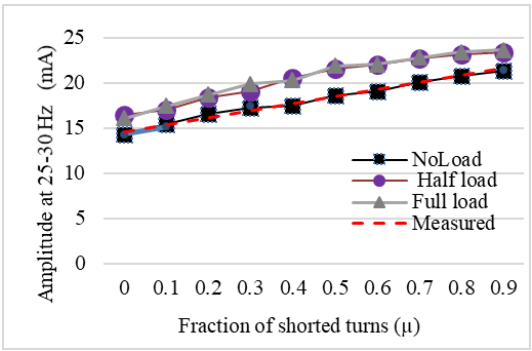

(c) MULLER OY714

Figure 9. Variation of amplitude at 25 Hz with fraction of shorted turns, from model and experimentally tested motor

in the phase A with varying load conditions. Figure 9 (a) shows the frequency spectrum of simulated and measured current of phase A with 50 % stator shorted turns on testing the 0.37 kW induction motor.

On the other hand, Figure 9 (b) and Figure 9 (c) show the stator current amplitude versus the fraction of shorted turns (μ) from measurements and simulations of the 2.2 kW and 0.37 kW induction motors. In this result, the modeling of inter-turn short circuit used motor specification and the percentage of winding shorted. The short circuit frequencies and amplitudes are sufficiently developed. When objective comparison is performed between the healthy and stator fault conditions, the proportional amplitude of the harmonic increased as the percentage of shorted winding increased.

Table 2 shows the error comparison between accurate measurement and model simulation. It is observed that the accuracy in the model simulation is more than 96 %. The results in this experiment for small commercial induction motors did not cover large and expensive motors that have high maintenance costs.

5. Conclusions

Detection of stator winding inter-turn fault at a developing stage is extremely important in an industrial system. This paper provides a simple, fast, yet efficient technique for direct detection by DQ state-space model-based analysis, demonstrated using MATLAB/Simulink. This paper presents a model-based design of the induction motor with inter-turn shorted winding fault.

The transient and steady-state behaviors of an induction motor can be described by its state space DQ model. The machine is modeled in such a way that certain ideas about the equations and the subsystems are clearly shown using MATLAB/Simulink. In addition to this, a faulty motor that has shorted stator turns is also modeled and compared for variations in torque and current waveforms.

The results from model simulations and from laboratory tests with 0.37 kW and 2.2 kW three-phase induction motors were in a good agreement, with various percentages of the turns shorted. The model enables diagnostic fault detection algorithms to operate in real time.

The developed model was effective in accurately simulating the harmonic current in the induction motor, and accurately reflected experiments with a real induction motor. The results confirm that the proposed DQ state space model allows the magnitude of faulty winding to be estimated precisely. Based on the proposed model, various applications can be developed to achieve fault monitoring and detection systems for induction motors.

Acknowledgements

This work has been financially supported by the Faculty of Engineering at Prince of Songkla University, with Graduate Studies Grant.

References

Accetta, A., Cirrincione, M., Pucci, M., & Sferlazza, A. (2020). State space-vector model of linear induction motors including end-effects and iron losses Part I: Theoretical analysis. *IEEE Transactions on Industry Applications*, *56*(1), 235–244. doi:10.1109/TIA.2019.2952031

Berzoy, A., Mohamed, A. A. S., & Mohammed, O. (2017). Impact of inter-turn short-circuit location on induction machines parameters through FE computations. *IEEE Transactions on Magnetics*, *53*(6), 1–4. doi:10.1109/TMAG.2017.2665639

Boglietti, A., Cossale, M., Vaschetto, S., & Dutra, T. (2018). Winding thermal model for short-time transient: Experimental validation in operative conditions. *IEEE Transactions on Industry Applications*, *54*(2), 1312–1319. doi:10.1109/TIA.2017.2777920

Deeb, M., Kotelenets, N. F., Assaf, T., Sultan, H. M., & akaysheedept, A. S. A. (2021). Three-phase induction motor short circuits fault diagnosis using MCSA and NSC. *Proceedings of the 3rd International Youth Conference on Radio Electronics, Electrical and Power Engineering (REEPE) 2021*, 1–6. doi:10.1109/REEPE51337.2021.9388051

Faiz, J., Keravand, M., Ghasemi-Bijan, M., Cruz, S. M. Â., & Bandar-Abadi, M. (2016). Impacts of rotor inter-turn short circuit fault upon performance of wound rotor induction machines. *Electric Power Systems Research*, *135*, 48–58. doi:10.1016/j.epsr.2016.03.007

Gurusamy, V., Bostanci, E., Li, C., Qi, Y., & Akin, B. (2021). A stray magnetic flux-based robust diagnosis method for detection and location of interturn short circuit fault in pmsm. *IEEE Transactions on Instrumentation and Measurement*, *70*, 1–11. doi:10.1109/TIM.2020.3013128

Kocman, S., & Nowak, S. (2019). Analysis of the stator winding fault of induction motor using COMSOL multiphysics. *Proceedings of the 20th International Scientific Conference on Electric Power Engineering (EPE) 2019*, 1–6. doi:10.1109/EPE.2019.8778128

Lv, G., Zeng, D., & Zhou, T. (2018). An advanced equivalent circuit model for linear induction motors. *IEEE Transactions on Industrial Electronics*, *65*(9), 7495–7503. doi:10.1109/TIE.2018.2807366

Meserkhani, A., Jafari, S. M., & Rahi, A. (2021). Experimental comparison of acoustic emission sensors in the detection of outer race defect of angular contact ball bearings by artificial neural network. *Measurement*, *168*, 108198. doi:10.1016/j.measurement.2020.108198

Ojaghi, M., & Daliri, S. (2017). Analytic model for performance study and computer-aided design of single-phase shaded-pole induction motors. *IEEE Transactions on Energy Conversion*, *32*(2), 649–657. doi:10.1109/TEC.2016.2645641

Pucci, M. (2019). State-space space-vector model of the induction motor including magnetic saturation and iron losses. *IEEE Transactions on Industry Applications*, *55*(4), 3453–3468. doi:10.1109/TIA.2019.2902327

Saddam, B., Ahmed, B. S., Aissa, A., & Ali, T. (2019). Squirrel cage induction motor under stator and rotor bars faults modeling and diagnosis. *Proceedings of the International Conference on Communications and Electrical Engineering, ICCEE 2018*. doi:10.1109/CCEE.2018.8634502

Shaikh, M. F., Park, J., & Lee, S. B. (2021). A non-intrusive leakage flux based method for detecting rotor faults in the starting transient of salient pole synchronous motors. *IEEE Transactions on Energy Conversion*, *36*(2), 1262–1270. doi:10.1109/TEC.2020.3021207

Shifat, T. A., & Hur, J. (2020). An improved stator winding short-circuit fault diagnosis using adaboost algorithm. *Proceedings of the International Conference on Artificial Intelligence in Information and Communication (ICAIIC)*, 382–387. doi:10.1109/ICAIIC48513.2020.9065081

Singh, A., Grant, B., DeFour, R., Sharma, C., & Bahadoorsingh, S. (2016). A review of induction motor fault modeling. *Electric Power Systems Research*, *133*, 191–197. doi:10.1016/j.epsr.2015.12.017

Verma, A. K., Akkulu, P., Padmanabhan, S. V., & Radhika, S. (2021). Automatic condition monitoring of industrial machines using fsa-based hall-effect transducer. *IEEE Sensors Journal*, *21*(2), 1072–1081. doi:10.1109/JSEN.2020.2990727